


Observation of flat and weakly dispersing bands in the van der Waals semiconductor math xmlns="http://www.w3.org/1998/Math/MathML">msub>mrow>mi>Nb/mi>/mrow>mn>3/mn>/msub>msub>mrow>mi>Br/mi>/mrow>mn>8/mn>/msub>/math> with breathing kagome lattice

Sabin Regmi, Anup Pradhan Sakhya, Tharindu Fernando, Yuzhou Zhao, Dylan Jeff, Milo Sprague, Favian Gonzalez, Iftakhar Bin Elius, Mazharul Islam Mondal, Nathan Valadez, Damani Jarrett, Alexis Agosto, Jihui Yang, Jiun-Haw Chu, Saiful I. Khondaker, Xiaodong Xu, Ting Cao, and Madhab Neupane

Phys. Rev. B **108**, L121404 — Published 8 September 2023

DOI: 10.1103/PhysRevB.108.L121404

Observation of flat and weakly dispersing bands in a van der Waals semiconductor Nb_3Br_8 with breathing kagome lattice

Sabin Regmi,[1] Anup Pradhan Sakhya,[1] Tharindu Fernando,[2] Yuzhou Zhao,[2] Dylan Jeff,[1,3] Milo Sprague,[1] Favian Gonzalez,[1,3] Iftakhar Bin Elius,[1] Mazharul Islam Mondal,[1] Nathan Valadez,[1] Damani Jarrett,[1] Alexis Agosto,[1] Jihui Yang,[4] Jiun-Haw Chu,[2] Saiful I. Khondaker,[1,3] Xiaodong Xu,[2] Ting Cao,[4] and Madhab Neupane[1,*]

[1] *Department of Physics, University of Central Florida, Orlando, Florida 32816, USA*
[2] *Department of Physics, University of Washington, Seattle, Washington 98195, USA*
[3] *NanoScience and Technology Center, University of Central Florida, Orlando, Florida 32826, USA*
[4] *Department of Materials Science and Engineering, University of Washington, Seattle, Washington 98195, USA*

Niobium halides, Nb_3X_8 (X = Cl, Br, I), which are predicted two-dimensional magnets, have recently gotten attention due to their breathing kagome geometry. Here, we have studied the electronic structure of Nb_3Br_8 by using angle-resolved photoemission spectroscopy (ARPES) and first-principles calculations. ARPES results depict the presence of multiple flat and weakly dispersing bands. These bands are well explained by the theoretical calculations, which show they have Nb d character indicating their origination from the Nb atoms forming the breathing kagome plane. This van der Waals material can be easily thinned down via mechanical exfoliation to the ultrathin limit and such ultrathin samples are stable as depicted from the time-dependent Raman spectroscopy measurements at room temperature. These results demonstrate that Nb_3Br_8 is an excellent material not only for studying breathing kagome induced flat band physics and its connection with magnetism, but also for heterostructure fabrication and for practical application.

Quantum materials with kagome lattice - a geometry of six triangles sharing the corners to form a hexagon within - in their crystal structure have been recently studied as the potential playgrounds for exploring the interplay among parameters such as geometry, topology, electronic correlations, magnetic and charge density orders [1–12]. From the electronic structure point of view, a kagome lattice may support the presence of flat band, Dirac fermion, and saddle point with van Hove singularity. Angle resolved photoemission spectroscopy (ARPES) [13–15] has been successfully utilized to experimentally reveal some or all of these features in different kagome materials [7, 8, 10, 16–27]. Majority of the reports have been on kagome systems with conventional kagome geometry, where bond lengths between the ions forming such geometry is equal so that the size of all the triangles is same. Kagome lattice can occur in a different geometry called the breathing kagome, where alternating triangles have different bond length between the constituent ions leading to different size [28–30]. This difference may induce local electric dipole resulting in a ferroelectric order [31]. Although it has been theoretically predicted that the breathing kagome systems can host intrinsically robust flat bands [30] and higher-order topology [29], the experimental study of the breathing kagome systems for their electronic structure have been getting the attention only very recently [32–35].

Niobium halides Nb_3X_8 (X = Cl, Br, I) [36], which possess breathing kagome plane formed by the Nb atoms, present themselves as material platforms to investigate the interplay of the breathing kagome geometry with magnetism and electronic correlations in both three- and two-dimensional limits. These compounds exhibit some intriguing attributes that are advantageous for optoelectronic and nanodevice applications [37, 38]. They are moderate band gap semiconductors [33, 39] and in the monolayer form, they are predicted ferromagnet candidates [37, 40, 41]. The introduction of additional layers to the monolayer is predicted to lead to an antiferromagnetic ordering [40]. Importantly, because of very weak van der Waals coupling, they have very low exfoliation energies [38]. Therefore, obtaining the monolayers of these compounds is easily possible with mechanical exfoliation of the bulk crystals [33, 34, 39, 42, 43], which is beneficial for the fabrication of heterostructures. Very recently, Nb_3Br_8 has been used to fabricate a heterostructre with $NbSe_2$ to form a Josephson junction that can control the direction of current without the need of magnetic field [44]. Bulk Nb_3Br_8 is in the singlet magnetic ground state at room temperature [45]. Although the density functional theory (DFT)-based computations have been performed to predict the band structure of the monolayer of this compound [37], experimental demonstration of the electronic structure is still lacking.

In this letter, by means of ARPES measurements and supportive DFT computations, we report the electronic structure of Nb_3Br_8. The results of the ARPES measurements are consistent with the semiconducting nature of the material and the computed band structures well reproduce the experimental observations. Multiple flat and weakly dispersing bands are observed in the electronic band structure. The orbital-resolved calculations suggest these bands to have Nb d character indicative of

* Corresponding author: madhab.neupane@ucf.edu

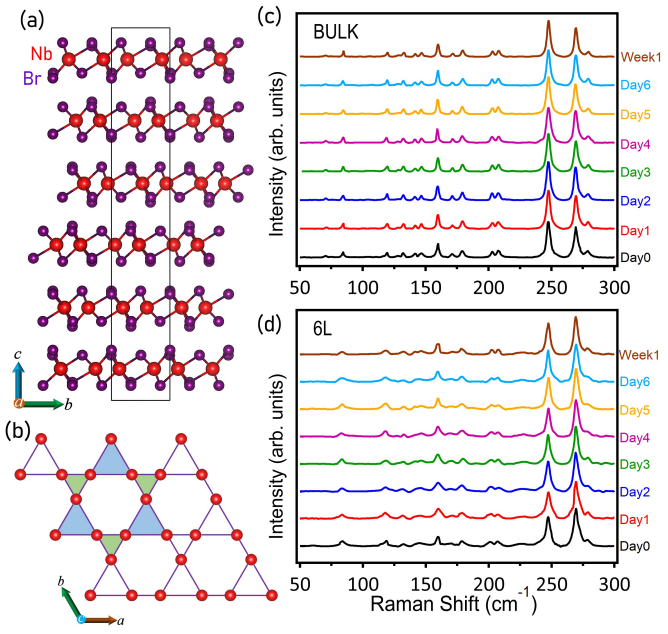

Fig. 1. Crystal structure and Raman spectroscopy measurements. (a) Crystal structure of Nb_3Br_8. Red and purple balls represent Nb and Br atoms, respectively. (b) Breathing kagome plane of Nb atoms. Up triangles (light blue) and down triangles (light green) have different bond lengths. (c,d) Time dependent Raman spectra of bulk and 6L Nb_3Br_8, respectively.

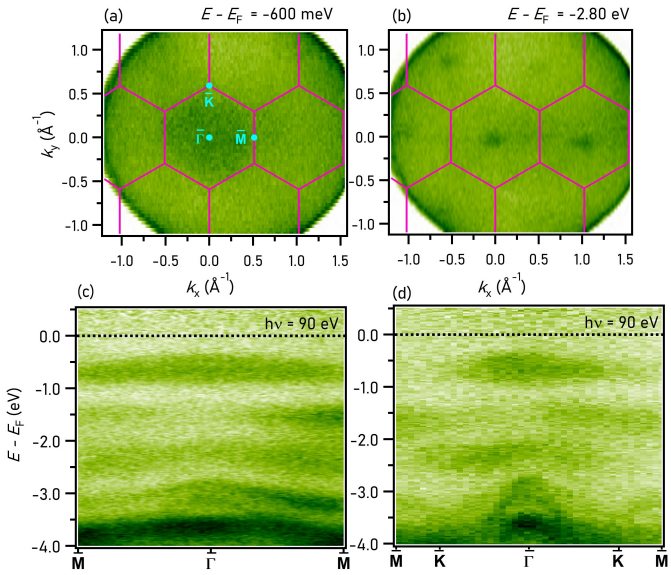

Fig. 2. Energy contours and band dispersion along different high-symmetry directions. (a,b) Energy contours measured by ARPES at the noted binding energies of −600 meV and −2.8 eV, respectively. (c-d) Experimental band structures along $\overline{M} - \overline{\Gamma} - \overline{M}$ and $\overline{M} - \overline{K} - \overline{\Gamma} - \overline{K} - \overline{M}$.

the origination from the breathing kagome plane of Nb atoms. Moreover, through mechanical exfoliation of bulk crystal, a thin 6L sample of this material has been obtained and the stability of the sample in its ultrathin limit has been demonstrated through time-dependent room-temperature Raman spectroscopy measurements. This study highlights Nb_3Br_8 as an excellent material candidate from both physics and application points of view by revealing the occurrence of flat band physics originating from breathing kagome lattice and by demonstrating an easy exfoliation of ultrathin sample and its stability at room temperature.

High-quality single crystals of Nb_3Br_8 used for this study were grown by using the chemical vapor transport method. The crystal structure and the chemical composition were checked by using X-ray diffraction and energy dispersive X-ray spectroscopy. The ARPES studies on these crystals were carried out at the Stanford Synchrotron Radiation Lightsource endstation 5-2, which is equipped with a DA30 analyzer. DFT [46, 47]-based first-principles computational results were implemented in the VASP package with Projector Augmented Wave pseudopotential [48–50]. The mid band-gap is set to be the zero-energy level for comparison with the experimental results. Hubbard potential $U = 1$ eV on Nb d orbitals is used to address the effects of on-site Coulomb interactions. Details on the experimental and computational methods have been provided in the supplemental material (SM) section I [51].

Nb_3Br_8 is a van der Waals layered material that crystallizes in rhombohedral space group $R\overline{3}m$ (# 166) with lattice parameters $a = b = 7.080$ Å and $c = 38.975$ Å [36]. As shown in Fig. 1(a), a bulk unit cell is composed of six monolayers of Nb_3Br_8, where the neighboring layers are connected through a very weak van der Waals interaction along crystallographic c-axis. In each layers, Nb atoms are arranged in a two-dimensional plane with breathing kagome geometry [Fig. 1(b)] and are sandwiched in between the bi-layers of Br atoms on either sides. Because of the weak van der Waals coupling, the crystals are easily cleavable along the (0001) direction. The ab-plane orientation of the cleaved surface is indicated by the observation of sharp (000l) peaks in the single-crystal X-ray diffraction pattern [see Fig. S1 in the SM [51]]. Importantly, bulk crystals can be easily exfoliated to ultrathin limits mechanically. We have thinned down the bulk crystal by using mechanical exfoliation to obtain a 6L Nb_3Br_8 [see Fig. S2 in the SM [51]]. In Fig. 1(c), we present the results of the Raman spectroscopy measurements carried out on bulk and the 6L thin Nb_3Br_8. Tracking the evolution of the Raman spectra over time in Fig. 1(c-d), it is observed that the Raman modes do not experience shifts in peak frequency, changes in peak intensity, or peak broadening in either the bulk or 6L data. The absence of these changes in the Raman spectra signifies that the crystals are retaining good crystallinity throughout, speaking to the stability of the material in both bulk and thin layers. The fact that

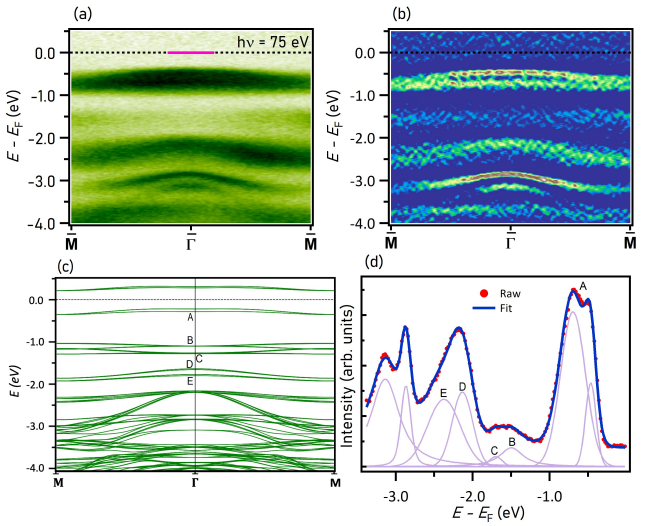

Fig. 3. Experimental and theoretical $\overline{\mathrm{M}}-\overline{\Gamma}-\overline{\mathrm{M}}$ band dispersion. (a) Band dispersion along $\overline{\mathrm{M}}-\overline{\Gamma}-\overline{\mathrm{M}}$ measured using incident photon energy of 75 eV and (b) its second derivative plot. (c) Calculated band structure along M−Γ−M. (d) EDC integrated within a momentum window of (−0.1 /Å, 0.1 /Å) represented by the magneta line in (a) and its voigt fit.

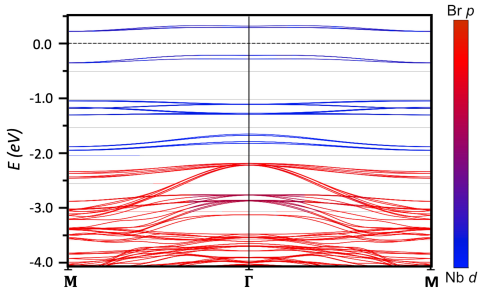

Fig. 4. Computed contribution of Nb d and Br p in the band structure along $\mathrm{M}-\Gamma-\mathrm{M}$.

the crystal structure of Nb_3Br_8 is stable within a week's time is promising for the future application of the material in technology or further research of its fundamental properties. Recent magnetic susceptibility study reports that the bulk Nb_3Br_8 undergoes a magnetic transition to a singlet state at around 382 K [45]. Our magnetic susceptibility measurement [see Fig. S1 in the SM [51]] shows an abrupt jump at a temperature of around 394 K, which is slightly off the reported transition temperature.

The results of ARPES and accompanying first-principles band structure calculations are presented in Figs. 2-4, with a aim to unveil the electronic structure and the potential presence flat bands arising from the breathing kagome geometry in the crystal structure. The energy contours obtained from APRES measurement with 90 eV incident photon energy at binding energies of −0.6 eV and −2.8 eV are presented in Figs. 2(a) and 2(b), respectively. Consistent with the semiconducting nature of the material, no photoemission signal is obtained at the Fermi level. While a clear photoemission intensity can be visualized in the −0.6 eV energy contour [Fig. 2(a)], a hexagonal pattern, typical of kagome systems, can be seen in the −2.8 eV energy contour [Fig. 2(b)]. In order to reveal the underlying band structure along different high-symmetry directions, we took dispersion maps along the $\overline{\mathrm{M}}-\overline{\Gamma}-\overline{\mathrm{M}}$ and $\overline{\mathrm{M}}-\overline{\mathrm{K}}-\overline{\Gamma}-\overline{\mathrm{K}}-\overline{\mathrm{M}}$ directions. The high-symmetry points are marked in Fig. 2(a). The band structures along these high-symmetry directions seem to reveal similar features. Also, similar results have been obtained for different photon energies of the incident light [see FIG. S3 in the SM [51]].

Figures 3(a-b) show energy-momentum dispersion along $\overline{\mathrm{M}}-\overline{\Gamma}-\overline{\mathrm{M}}$ measured with a photon enrgy of 75 eV and its second derivative plot, respectively. These plots show the presence of multiple flat and weakly dispersing bands within −2.5 eV binding energy. In Fig. 3(c), we present the calculated band structure along the M−Γ−M direction. The calculated band structure seems to reproduce the experimental observations quite well [See Fig. S4 in the SM [51] for comparison of experimental and calculated band dispersion along $\overline{\mathrm{M}}-\overline{\mathrm{K}}-\overline{\Gamma}-\overline{\mathrm{K}}-\overline{\mathrm{M}}$]. For the comparison with the experimental results, the mid-bandgap in the calculation has been set to zero. We can see that the energy positions of the bands in experimental and calculations results do not match. This discrepancy might arise due to various factors such as the underestimation of the bandgap by DFT or the sample not being perfectly stoichiometric. Nevertheless, the calculated band structure shows the presence of bandsets - labelled A → E - within 2 eV below the Fermi level. The bandset A has two almost flat and parallel bands near the Γ point, among which the upper one seems to weakly disperse away from Γ before merging together near the M point. These bands can be seen in the dispersion map in Fig. 3(a) and better visualized in its second derivative [Fig. 3(b)]. Near the center of the BZ, these bands are almost flat and form a gap, which narrows down going towards the M point at which they seem to meet each other. Similarly, bandsets B and C both consist of two flat bands, one of which seems to separate and become dispersive going away from the Γ point. The bands within the bandsets B and C are hard to distinguish in the experimental dispersion map as they form a wide spectrum of intensity that gives rise to a flat feature centered around 1.6 eV [see Figs. 3(a)]. In Fig. 3(d), we present the energy distribution curve (EDC) integrated within a momentum window of (−0.1 /Å, 0.1 /Å) represented by the magenta line in the raw dispersion map in Fig. 3(a). Several intensity peaks corresponding to the presence of bands can be observed. In particular, a two-peak feature centered around −0.6 eV can be observed, which corresponds to the pair of almost flat bands (bandset A). By fitting the raw EDC data with voigt functions, we obtain that these almost flat bands in the bandset A are located around −0.46 eV and −0.70 eV binding energies, respectively. Another broad but much

suppressed intensity feature can be observed centered around 1.6 eV binding energy in the EDC, which corresponds to the observed flat dispersion in Fig. **3**(a). A good fitting is obtained by considering presence of two peaks located around −1.5 eV and −1.7 eV binding energies. For both bandsets B and C, as the flat band and the flat region of the other band dispersing away from $\overline{\Gamma}$ merge together near the center of the BZ, they appear as these single peaks in the intensity plot within the experimental resolution. Fitting the EDC integrated within ($\overline{\mathrm{M}}$, $\overline{\mathrm{M}} - 0.1$ Å^{-1}), where these bands seem to get separated, shows the presence of a pair of bands in each of the bandsets B and C [see the Fig. S5 in the SM [51]]. Below C, there exist a relatively dispersive bandset D and a weakly dispersing bandset E, which are centered around 2.13 eV and 2.37 eV near the $\overline{\Gamma}$ point in the experimental data [Fig. **3**(d)].

The measurements at varying photon energies show that the aforementioned flat and weakly dispersing bands seem to have fairly similar dispersion irrespective of the choice of the photon energy indicative of their origination from two-dimensional plane [see the Fig. S3 in the SM [51] for photon energy dependent measurements]. To understand if the origination of the flat and dispersing bands is from the breathing kagome plane of Nb atoms, we plot in Fig. **4** the contribution of Nb d and Br p in the electronic structure along M−Γ−M. While the dispersive bands deep below the Fermi level have Br p character, it can be seen that the frontier flat and weakly dispersing bands discussed above have Nb d character [see Fig. S8 in the SM [51] for individual Nb d orbitals' contribution]. This confirms that the Nb atoms, which configure themselves in the breathing kagome geometry, give rise to these flat and weakly dispersing bands. Nb_3Br_8 is a predicted ferromagnet in its monolayer form [37]. To see how the band structure in the two-dimensional form will compare with the band structure of the bulk, we computed ferromagnetic band structure calculations for the monolayer [see Fig. S6 in the SM [51]]. From the comparison, we anticipate that the frontier electronic band structure for thin samples and bulk will look similar overall.

To conclude, the electronic structure of the niobium halide semiconductor Nb_3Br_8 has been studied by using ARPES and first-principles calculations. In its crystal structure, Nb atoms form a breathing kagome lattice with different Nb–Nb bond lengths in alternate triangles. Experimental dispersion maps reveal the presence of multiple weakly dispersing and flat bands, with the highest set of such bands occurring around 460 and 700 meV below the Fermi level. The comparison with the first-principles computations show that these flat and weakly dispersing bands have Nb − d character suggesting their origination from the breathing kagome plane formed by the Nb atoms. Room temperature Raman measurements on a 6L sample mechanically exfoliated from the bulk crystal depict the stability of the ultra-thin sample suggesting Nb_3Br_8 as an excellent ground to study breathing kagome geometry induced flat band physics and its application.

M. N. acknowledges the support from the National Science Foundation (NSF) CAREER award DMR-1847962, the NSF Partnerships for Research and Education in Materials (PREM) Grant DMR-2121953, and the Air Force Office of Scientific Research MURI Grant No. FA9550-20-1-0322. T. C. and X. X. acknowledge the support from UW Molecular Engineering Materials Center, a NSF Materials Research Science and Engineering Center (Grant No. DMR-1719797). S.I.K. also acknowledges the support from the NSF PREM Grant DMR-2121953. This study uses the resources of the Stanford Synchrotron Radiation Lightsource (SSRL), SLAC National Accelerator Laboratory, which is supported by the U.S. Department of Energy, Office of Science, Office of Basic Energy Sciences under Contract No. DE-AC02-76SF00515. We acknowledge the beamline assistance from Dr. Makoto Hashimoto and Dr. Donghui Lu at SSRL.

[1] S.-L. Yu and J.-X. Li, Chiral superconducting phase and chiral spin-density-wave phase in a Hubbard model on the kagome lattice, Phys. Rev. B **85**, 144402 (2012).
[2] M. L. Kiesel and R. Thomale, Sublattice interference in the kagome Hubbard model, Phys. Rev. B **86**, 121105 (2012).
[3] T.-H. Han, J. S. Helton, S. Chu, D. G. Nocera, J. A. Rodriguez-Rivera, C. Broholm, and Y. S. Lee, Fractionalized excitations in the spin-liquid state of a kagome-lattice antiferromagnet, Nature **492**, 406 (2012).
[4] W.-S. Wang, Z.-Z. Li, Y.-Y. Xiang, and Q.-H. Wang, Competing electronic orders on kagome lattices at van Hove filling, Phys. Rev. B **87**, 115135 (2013).
[5] M. L. Kiesel, C. Platt, and R. Thomale, Unconventional Fermi Surface Instabilities in the Kagome Hubbard Model, Phys. Rev. Lett. **110**, 126405 (2013).
[6] I. I. Mazin, H. O. Jeschke, F. Lechermann, H. Lee, M. Fink, R. Thomale, and R. Valentí, Theoretical prediction of a strongly correlated Dirac metal, Nat. Commun. **5**, 4261 (2014).
[7] Z. Lin, J.-H. Choi, Q. Zhang, W. Qin, S. Yi, P. Wang, L. Li, Y. Wang, H. Zhang, Z. Sun, L. Wei, S. Zhang, T. Guo, Q. Lu, J.-H. Cho, C. Zeng, and Z. Zhang, Flatbands and Emergent Ferromagnetic Ordering in Fe_3Sn_2 Kagome Lattices, Phys. Rev. Lett. **121**, 096401 (2018).
[8] L. Ye, M. Kang, J. Liu, F. von Cube, C. R. Wicker, T. Suzuki, C. Jozwiak, A. Bostwick, E. Rotenberg, D. C. Bell, L. Fu, R. Comin, and J. G. Checkelsky, Massive Dirac fermions in a ferromagnetic kagome metal, Nature **555,** 638 (2018).
[9] J.-X. Yin, S. S. Zhang, G. Chang, Q. Wang, S. S. Tsirkin, Z. Guguchia, B. Lian, H. Zhou, K. Jiang, I. Belopolski, N. Shumiya, D. Multer, M. Litskevich, T. A. Cochran, H. Lin, Z. Wang, T. Neupert, S. Jia, H. Lei, and M.

Z. Hasan, Negative flat band magnetism in a spin–orbit-coupled correlated kagome magnet, Nat. Phys. **15**, 443 (2019).
[10] J.-X. Yin, W. Ma, T. A. Cochran, X. Xu, S. S. Zhang, H.-J. Tien, N. Shumiya, G. Cheng, K. Jiang, B. Lian, Z. Song, G. Chang, I. Belopolski, D. Multer, M. Litskevich, Z.-J. Cheng, X. P. Yang, B. Swidler, H. Zhou, H. Lin, T. Neupert, Z. Wang, N. Yao, T.-R. Chang, S. Jia, and M. Zahid Hasan, Quantum-limit Chern topological magnetism in $TbMn_6Sn_6$, Nature **583**, 533 (2020).
[11] Z. Lin, C. Wang, P. Wang, S. Yi, L. Li, Q. Zhang, Y. Wang, Z. Wang, H. Huang, Y. Sun, Y. Huang, D. Shen, D. Feng, Z. Sun, J.-H. Cho, C. Zeng, and Z. Zhang, Dirac fermions in antiferromagnetic FeSn kagome lattices with combined space inversion and time-reversal symmetry, Phys. Rev. B **102,** 155103 (2020).
[12] N. J. Ghimire, R. L. Dally, L. Poudel, D. C. Jones, D. Michel, N. T. Magar, M. Bleuel, M. A. McGuire, J. S. Jiang, J. F. Mitchell, J. W. Lynn, and I. I. Mazin, Competing magnetic phases and fluctuation-driven scalar spin chirality in the kagome metal YMn_6Sn_6, Sci. Adv. **6**, eabe2680 (2020).
[13] A. Damascelli, Z. Hussain, and Z.-X. Shen, Angle-resolved photoemission studies of the cuprate superconductors, Rev. Mod. Phys. **75**, 473 (2003).
[14] A. Damascelli, Probing the Electronic Structure of Complex Systems by ARPES, Phys. Scr. **2004**, 61 (2004).
[15] B. Lv, T. Qian, and H. Ding, Angle-resolved photoemission spectroscopy and its application to topological materials, Nat. Rev. Phys. **1**, 609 (2019).
[16] M. Kang, L. Ye, S. Fang, J.-S. You, A. Levitan, M. Han, J. I. Facio, C. Jozwiak, A. Bostwick, E. Rotenberg, M. K. Chan, R. D. McDonald, D. Graf, K. Kaznatcheev, E. Vescovo, D. C. Bell, E. Kaxiras, J. van den Brink, M. Richter, M. Prasad Ghimire, J. G. Checkelsky, and R. Comin, Dirac fermions and flat bands in the ideal kagome metal FeSn, Nat. Mater. **19**, 163 (2020).
[17] Z. Liu, M. Li, Q. Wang, G. Wang, C. Wen, K. Jiang, X. Lu, S. Yan, Y. Huang, D. Shen, J.-X. Yin, Z. Wang, Z. Yin, H. Lei, and S. Wang, Orbital-selective Dirac fermions and extremely flat bands in frustrated kagome-lattice metal CoSn, Nat. Commun. **11**, 4002 (2020).
[18] M. Kang, S. Fang, L. Ye, H. C. Po, J. Denlinger, C. Jozwiak, A. Bostwick, E. Rotenberg, E. Kaxiras, J. G. Checkelsky, and R. Comin, Topological flat bands in frustrated kagome lattice CoSn, Nat. Commun. **11**, 4004 (2020).
[19] B. R. Ortiz, S. M. L. Teicher, Y. Hu, J. L. Zuo, P. M. Sarte, E. C. Schueller, A. M. M. Abeykoon, M. J. Krogstad, S. Rosenkranz, R. Osborn, R. Seshadri, L. Balents, J. He, and S. D. Wilson, CsV_3Sb_5: A $\mathbb{Z}_2$ Topological Kagome Metal with a Superconducting Ground State, Phys. Rev. Lett. **125**, 247002 (2020).
[20] M. Li, Q. Wang, G. Wang, Z. Yuan, W. Song, R. Lou, Z. Liu, Y. Huang, Z. Liu, H. Lei, Z. Yin, and S. Wang, Dirac cone, flat band and saddle point in kagome magnet YMn_6Sn_6, Nat. Commun. **12**, 3129 (2021).
[21] G. Dhakal, F. Cheenicode Kabeer, A. K. Pathak, F. Kabir, N. Poudel, R. Filippone, J. Casey, A. Pradhan Sakhya, S. Regmi, C. Sims, K. Dimitri, P. Manfrinetti, K. Gofryk, P. M. Oppeneer, and M. Neupane, Anisotropically large anomalous and topological Hall effect in a kagome magnet, Phys. Rev. B **104**, L161115 (2021).
[22] S. Peng, Y. Han, G. Pokharel, J. Shen, Z. Li, M. Hashimoto, D. Lu, B. R. Ortiz, Y. Luo, H. Li, M. Guo, B. Wang, S. Cui, Z. Sun, Z. Qiao, S. D. Wilson, and J. He, Realizing Kagome Band Structure in Two-Dimensional Kagome Surface States of RV_6Sn_6 (R = Gd, Ho), Phys. Rev. Lett. **127**, 266401 (2021).
[23] F. Kabir, R. Filippone, G. Dhakal, Y. Lee, N. Poudel, J. Casey, A. P. Sakhya, S. Regmi, R. Smith, P. Manfrinetti, L. Ke, K. Gofryk, M. Neupane, and A. K. Pathak, Unusual magnetic and transport properties in $HoMn_6Sn_6$ kagome magnet, Phys. Rev. Materials **6**, 064404 (2022).
[24] X. Teng, L. Chen, F. Ye, E. Rosenberg, Z. Liu, J.-X. Yin, Y.-X. Jiang, J. S. Oh, M. Z. Hasan, K. J. Neubauer, B. Gao, Y. Xie, M. Hashimoto, D. Lu, C. Jozwiak, A. Bostwick, E. Rotenberg, R. J. Birgeneau, J.-H. Chu, M. Yi, and P. Dai, Discovery of charge density wave in a kagome lattice antiferromagnet, Nature **609**, 490 (2022).
[25] Y. Hu, X. Wu, Y. Yang, S. Gao, N. C. Plumb, A. P. Schnyder, W. Xie, J. Ma, and M. Shi, Tunable topological Dirac surface states and van Hove singularities in kagome metal GdV_6Sn_6, Sci. Adv. **8**, eadd2024 (2022).
[26] X. Gu, C. Chen, W. S. Wei, L. L. Gao, J. Y. Liu, X. Du, D. Pei, J. S. Zhou, R. Z. Xu, Z. X. Yin, W. X. Zhao, Y. D. Li, C. Jozwiak, A. Bostwick, E. Rotenberg, D. Backes, L. S. I. Veiga, S. Dhesi, T. Hesjedal, G. van der Laan, H. F. Du, W. J. Jiang, Y. P. Qi, G. Li, W. J. Shi, Z. K. Liu, Y. L. Chen, and L. X. Yang, Robust kagome electronic structure in the topological quantum magnets XMn_6Sn_6 (X = Dy, Tb, Gd, Y), Phys. Rev. B **105**, 155108 (2022).
[27] T. Y. Yang, Q. Wan, J. P. Song, Z. Du, J. Tang, Z. W. Wang, N. C. Plumb, M. Radovic, G. W. Wang, G. Y. Wang, Z. Sun, J.-X. Yin, Z. H. Chen, Y. B. Huang, R. Yu, M. Shi, Y. M. Xiong, and N. Xu, Fermi-level flat band in a kagome magnet, Quantum Front. **1**, 14 (2022).
[28] N. Hänni, M. Frontzek, J. Hauser, D. Cheptiakov, and K. Krämer, Low Temperature Phases of Na2Ti3Cl8 Revisited, Z. Anorg. Allg. Chem. **643**, 2063 (2017).
[29] M. Ezawa, Higher-Order Topological Insulators and Semimetals on the Breathing Kagome and Pyrochlore Lattices, Phys. Rev. Lett. **120**, 026801 (2018).
[30] A. Bolens and N. Nagaosa, Topological states on the breathing kagome lattice, Phys. Rev. B **99**, 165141 (2019).
[31] Y. Li, C. Liu, G.-D. Zhao, T. Hu, and W. Ren, Two-dimensional multiferroics in a breathing kagome lattice, Phys. Rev. B **104**, L060405 (2021).
[32] H. Tanaka, Y. Fujisawa, K. Kuroda, R. Noguchi, S. Sakuragi, C. Bareille, B. Smith, C. Cacho, S. W. Jung, T. Muro, Y. Okada, and T. Kondo, Three-dimensional electronic structure in ferromagnetic Fe_3Sn_2 with breathing kagome bilayers, Phys. Rev. B **101**, 161114 (2020).
[33] Z. Sun, H. Zhou, C. Wang, S. Kumar, D. Geng, S. Yue, X. Han, Y. Haraguchi, K. Shimada, P. Cheng, L. Chen, Y. Shi, K. Wu, S. Meng, and B. Feng, Observation of Topological Flat Bands in the Kagome Semiconductor Nb_3Cl_8, Nano Lett. **22**, 4596 (2022).
[34] S. Regmi, T. Fernando, Y. Zhao, A. P. Sakhya, G. Dhakal, I. Bin Elius, H. Vazquez, J. D. Denlinger, J. Yang, J.-H. Chu, X. Xu, T. Cao, and M. Neupane, Spectroscopic evidence of flat bands in breathing kagome semiconductor Nb_3I_8, Commun. Mater. **3**, 100 (2022).
[35] Shunye Gao, Shuai Zhang, Cuixiang Wang, Wei Tao, Jingtong Liu, Tiantian Wang, Shuaikang Yuan, Gexing Qu, Mojun Pan, Shiyu Peng, Yong Hu, Hang Li, Yaobo Huang, Hui Zhou, Sheng Meng, Liu Yang, Zhiwei Wang,

Yugui Yao, Zhiguo Chen, Ming Shi, Hong Ding, Kun Jiang, Yunliang Li, Youguo Shi, Hongming Weng, and T. Qian, Mott insulator state in a van der Waals flat-band compound, arXiv:2205.11462 (2022).

[36] S. N. Magonov, P. Zoennchen, H. Rotter, H. J. Cantow, G. Thiele, J. Ren, and M. H. Whangbo, Scanning tunneling and atomic force microscopy study of layered transition metal halides Nb_3X_8 (X = Cl, Br, I), J. Am. Chem. Soc. **115**, 2495 (1993).

[37] J. Jiang, Q. Liang, R. Meng, Q. Yang, C. Tan, X. Sun, and X. Chen, Exploration of new ferromagnetic, semiconducting and biocompatible Nb_3X_8 (X = Cl, Br or I) monolayers with considerable visible and infrared light absorption, Nanoscale **9**, 2992 (2017).

[38] B. Mortazavi, X. Zhuang, and T. Rabczuk, A first-principles study on the physical properties of two-dimensional Nb_3Cl_8, Nb_3Br_8 and Nb_3I_8. Appl. Phys. A **128**, 934 (2022).

[39] S. Oh, K. H. Choi, S. Chae, B. J. Kim, B. J. Jeong, S. H. Lee, J. Jeon, Y. Kim, S. S. Nanda, L. Shi, D. K. Yi, J.-H. Lee, H. K. Yu, and J.-Y. Choi, Large-area synthesis of van der Waals two-dimensional material Nb_3I_8 and its infrared detection applications, J. Alloys Compd. **831**, 154877 (2020).

[40] F. Conte, D. Ninno, and G. Cantele, Layer-dependent electronic and magnetic properties of Nb_3I_8, Phys. Rev. Res. **2**, 033001 (2020).

[41] G. Cantele, F. Conte, L. Zullo, and D. Ninno, Tunable electronic and magnetic properties of thin Nb_3I_8 nanofilms: Interplay between strain and thickness, Phys. Rev. B **106**, 085418 (2022).

[42] B. J. Kim, B. J. Jeong, S. Oh, S. Chae, K. H. Choi, S. S. Nanda, T. Nasir, S. H. Lee, K.-W. Kim, H. K. Lim, L. Chi, I. J. Choi, M.-K. Hong, D. K. Yi, H. K. Yu, J.-H. Lee, and J.-Y. Choi, Structural and Electrical Properties of Nb_3I_8 Layered Crystal, Phys. Status Solidi RRL **13**, 1800448 (2019).

[43] J. Yoon, E. Lesne, K. Sklarek, J. Sheckelton, C. Pasco, S. S. P. Parkin, T. M. McQueen, and M. N. Ali, Anomalous thickness-dependent electrical conductivity in van der Waals layered transition metal halide, Nb_3Cl_8, J. Phys. Condens. Mater. 32, 304004 (2020).

[44] H. Wu, Y. Wang, Y. Xu, P. K. Sivakumar, C. Pasco, U. Filippozzi, S. S. P. Parkin, Y.-J. Zeng, T. McQueen, and M. N. Ali, The field-free Josephson diode in a van der Waals heterostructure, Nature **604**, 653 (2022).

[45] C. M. Pasco, I. El Baggari, E. Bianco, L. F. Kourkoutis, and T. M. McQueen, Tunable Magnetic Transition to a Singlet Ground State in a 2D van der Waals Layered Trimerized Kagomé Magnet, ACS Nano **13**, 9457 (2019).

[46] P. Hohenberg and W. Kohn, Inhomogeneous Electron Gas, Phys. Rev. **136,** B864 (1964).

[47] W. Kohn and L. J. Sham, Self-Consistent Equations Including Exchange and Correlation Effects, Phys. Rev. **140,** A1133 (1965).

[48] G. Kresse and J. Furthmüller, Efficient iterative schemes for *ab initio* total-energy calculations using a plane-wave basis set, Phys. Rev. B **54**, 11169 (1996).

[49] G. Kresse and J. Furthmüller, Efficiency of ab-initio total energy calculations for metals and semiconductors using a plane-wave basis set, Comput. Mat. Sci. **6**, 15 (1996).

[50] G. Kresse and D. Joubert, From ultrasoft pseudopotentials to the projector augmented-wave method, Phys. Rev. B **59**, 1758 (1999).

[51] See the supplemental material for supporting information.